



ARTICLE

DOI: 10.1038/s41467-018-06319-6

OPEN

Vegetation response to exceptional global warmth during Oceanic Anoxic Event 2

Ulrich Heimhofer¹, Nina Wucherpennig¹, Thierry Adatte², Stefan Schouten^{3,4}, Elke Schneebeli-Hermann ⁵, Silvia Gardin⁶, Gerta Keller⁷, Sarah Kentsch¹ & Ariane Kujau ⁸

The Cenomanian–Turonian Oceanic Anoxic Event (OAE2; ~94.5 million years ago) represents an episode of global-scale marine anoxia and biotic turnover, which corresponds to one of the warmest time intervals in the Phanerozoic. Despite its global significance, information on continental ecosystem response to this greenhouse episode is lacking. Here we present a terrestrial palynological record combined with marine-derived temperature data (TEX₈₆) across an expanded OAE2 section from the Southern Provençal Basin, France. Despite high TEX₈₆-derived temperature estimates reaching up to 38 °C, the continental hinterland did support a diverse vegetation, adapted to persist under elevated temperatures. A transient phase of climatic instability and cooling during OAE2 known as Plenus Cold Event (PCE) is marked by the proliferation of open, savanna-type vegetation rich in angiosperms at the expanse of conifer-dominated forest ecosystems. A rise in early representatives of Normapolles-type pollen during the PCE marks the initial radiation of this important angiosperm group.

¹Institute for Geology, Leibniz Universität Hannover, 30167 Hannover, Germany. ²Institute of Geology and Palaeontology, Université de Lausanne, 1015 Lausanne, Switzerland. ³Royal Netherlands Institute for Sea Research (NIOZ), Department of Marine Microbiology and Biogeochemistry, Utrecht University, 1790 AB Den Burg, Texel, The Netherlands. ⁴Department of Earth Sciences, Utrecht University, 3584 CS Utrecht, The Netherlands. ⁵Paleontological Institute and Museum, Universität Zürich, 8006 Zürich, Switzerland. ⁶Centre de recherche sur la Paléobiodiversité et les Paléoenvironnements, Université Pierre et Marie Curie Paris 06, 75252 Paris, France. ⁷Department of Geosciences, Princeton University, Princeton 08544 NJ, USA. ⁸GFZ German Research Centre for Geosciences, Telegrafenberg 14473 Potsdam, Germany. Correspondence and requests for materials should be addressed to U.H. (email: heimhofer@geowi.uni-hannover.de)

Past time intervals of exceptional climatic warmth, typically associated with elevated $p\text{CO}_2$, had profound impacts on floral compositions and biogeographic patterns of continental vegetation^{1–3}. Within the overall greenhouse climate characterizing the Mesozoic, the Late Cretaceous Oceanic Anoxic Event (OAE) 2, which spans the Cenomanian–Turonian boundary [94.1 million years ago (Ma)], marks the onset of an extreme phase in ocean temperatures known as the “Cretaceous thermal maximum”^{4–6}. This phase is characterized by one of the highest (>35 °C) proxy data-derived sea-surface temperature (SST) estimates of the last 150 Myrs, which are recorded by both planktonic foraminifera $\delta^{18}\text{O}$ and archaeal membrane lipid-based TEX_{86} data⁶. A significant rise in low- and mid-latitude open ocean SSTs (2–4 °C) and mid-latitude shelf-sea temperatures (4–5 °C) accompanied the onset of OAE2, resulting in the Late Cenomanian–Turonian hothouse^{5,7–9}. Besides the exceptional thermal conditions, the OAE2 (lasting 700–800 kyrs^{10,11}) is associated with widespread formation of organic-rich deep-water deposits^{12,13}, a major positive carbon isotope excursion (CIE) in carbonate and organic carbon reflecting massive burial of ^{13}C -depleted carbon^{14,15}, and major biotic turnover in marine ecosystems^{16,17}.

Despite the outstanding position of OAE2 as one of the most remarkable events of the Mesozoic¹⁸, the responses of terrestrial ecosystems and continental flora to the changes of the global climate system remain largely unexplored. To date, just a few isolated plant macrofossil discoveries have been reported from the organic-rich Bonarelli Level, which is the sedimentary expression of the OAE2 in Marche–Umbria, Italy¹⁹. Microfloral evidence is essentially lacking due to the overwhelming predominance of amorphous kerogen in most marine OAE2 black shales, diluting any continent-derived spore-pollen signal. However, based on a shift in the $\delta^{13}\text{C}$ signature of leaf-wax n -alkanes, a change from C3 to C4-dominated low-latitude vegetation triggered by a $p\text{CO}_2$ drop has been proposed²⁰ for the early phase of OAE2. According to theoretical considerations²¹, the exceptional warmth that prevailed during Late Cenomanian–Turonian times may have exceeded the heat tolerance of continental ecosystems, which potentially resulted in widespread vegetation dieback.

Here we present a high resolution and taxonomically differentiated spore-pollen record across a stratigraphic interval correlating to the OAE2. The record is from an expanded marine section (Cassis) from the Southern Provençal Basin (SPB) of S' France (Fig. 1) and has been analyzed for biostratigraphy,

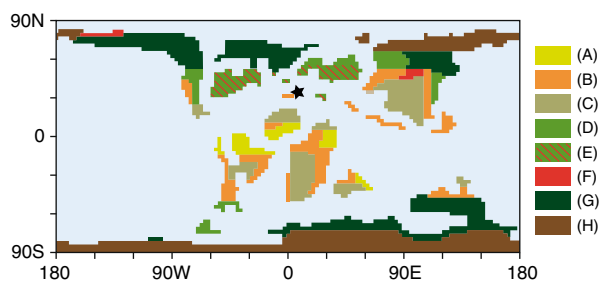


Fig. 1 Palaeogeographic map illustrating Cenomanian–Turonian biome distribution. Palaeo-map is modified after ref. 48 and includes the extent of the Normapolles palynofloral province²⁹. Color code representing (A) tropical moist, open canopy mixed forest with shrub understory; (B) savanna-type dry low understory with sparse trees; (C) deciduous dry/warm shrubland; (D) mid-latitude evergreen closed canopy conifer forest; (E) Normapolles province; (F) evergreen wet/cool shrubland; (G) high-latitude moist, open canopy forest with shrub understory; (H) boreal closed canopy conifer forest. Asterisk marks approximate location of the Southern Provençal Basin

palynology, TEX_{86} and stable carbon isotopic composition of carbonates and organic materials. Stratigraphic assignment of the section is based on existing ammonite data²² combined with new information from planktonic foraminifera, calcareous nannoplankton, and carbon isotopes of bulk carbonate, organic matter and plant wax-derived long-chain n -alkanes.

Results

Stratigraphy. The ~235 m thick Cassis section represents a heterolithic succession with its lowermost part being composed of clays and marls overlain by (in part) turbiditic sandstones (0.0–19.7 m). An exposure gap in the outcrop separates the siliclastic facies from a conspicuous limestone slope deposit characterized by intense slumping and disintegration (33.4–46.1 m). Above another exposure gap, the main part of the section is continuously accessible (55.8–236.0 m) and consists of homogenous marls with intercalated bundles of nodular limestone together representing basal facies. Existing ammonite data combined with new biostratigraphic results constrain this section to the Upper Cenomanian–Lower Turonian²² (Supplementary Note 1). This age assignment is further corroborated and refined by carbon isotope data, which show a characteristic positive CIE revealing an initial high-amplitude positive peak (a) followed by a trough interval, which gives way to a plateau with two consecutive peaks (b, c) (Fig. 2). The characteristic pattern of the CIE is mimicked in the $\delta^{13}\text{C}_{\text{org}}$ signature of bulk organic matter (Supplementary Fig. 1) and corroborated by the isotopic composition of long-chain n -alkanes derived from plant leaf-wax. Backed by high-resolution biostratigraphic data, the CIE evolution can be closely correlated with the reference carbon isotope record from Eastbourne, UK^{23,24} (Fig. 2). The significantly increased $\delta^{13}\text{C}_{\text{carb}}$ values of the CIE peak (a) at Cassis (6.0‰) compared to Eastbourne (4.8‰) may reflect a shift in the dominant carbonate source in the SPB during this particular interval. In fact, the Calcaires du Corton Fm. corresponds to a calcareous unit composed of upper slope deposits, which can be traced toward the shoalwater carbonate platform bordering the SPB to the north where similarly high $\delta^{13}\text{C}_{\text{carb}}$ signatures are observed in OAE2-equivalent platform limestones²⁵. Carbonate carbon isotope signatures > 6.0‰ for the OAE2 CIE are also described from the epicritic Iberian seaway²⁶ and may reflect variations in the aragonite content of the periplatform ooze exported from the adjacent platform²⁷. The correlation thus reveals very good stratigraphic coverage of the uppermost Cenomanian–Turonian at Cassis with an expanded ~200 m thick OAE2 interval (Fig. 2). High sedimentation rates accompanied by increased input of continental organic debris in a transtensive geotectonic setting²⁸ may have prevented the accumulation of black shales enriched in marine-derived organic carbon in the SPB.

Palynology. At Cassis, high numbers of inaperturate and bisaccate gymnosperm pollen (avg. = 48.2%) are essentially produced by Araucariaceae and Cupressaceae-type plants (*Araucariacites* spp.; *Inaperturopollenites* spp.) and Cheirolepidiaceae (*Classopollis* spp.) with subordinate contributions from Pinaceae (*Cerebropollenites* spp.) and Podocarpaceae (*Podocarpidites* spp.). Other gymnosperms, including cycads-ginkgophytes (*Cycadopsites* spp.), gnetaleans (*Ephedripites* spp.), and seed ferns (*Alisporites* spp.) are quantitatively of minor importance (avg. = 2.5%). Spores produced by a diverse assemblage of ground ferns and fern allies occur in moderate quantities (avg. = 12.8%). The assemblage contains a variety of eudicotyledonous angiosperm pollen represented by various tricolporate and triplicate types, the majority of which can be assigned to early forms of the

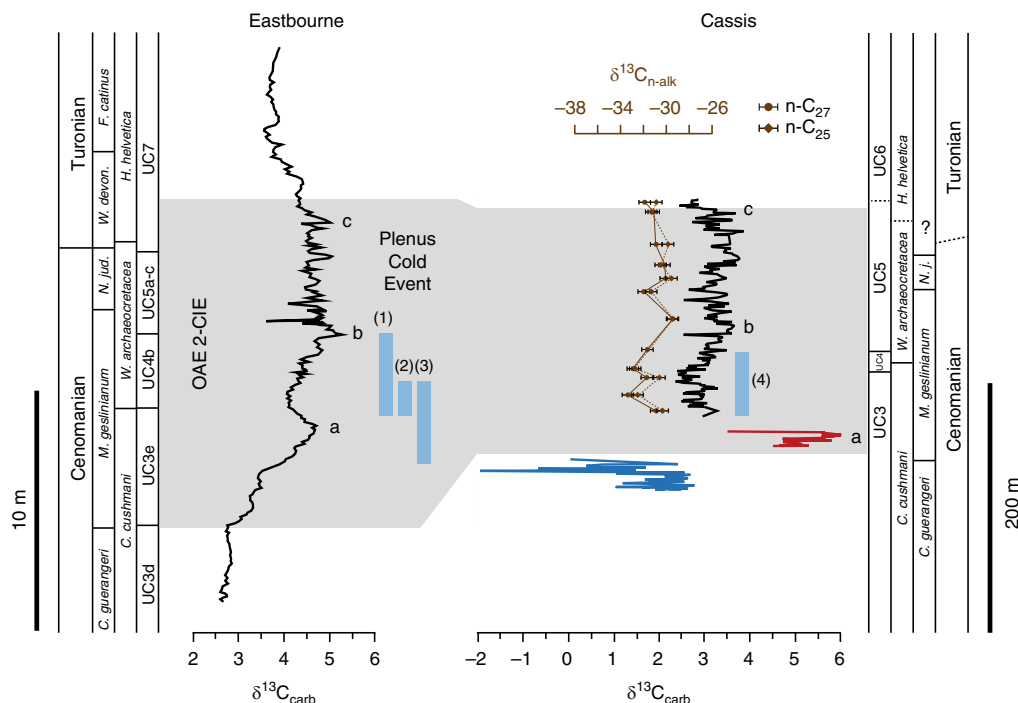


Fig. 2 Bio- and chemostratigraphic correlation. Carbon isotope trend from Cassis, S' France is compared with the European reference section at Eastbourne, Sussex, UK^{23,24}. Calcareous nannofossil zonation of Eastbourne after ref. ⁵⁶. Planktic foraminiferal biozonation of Eastbourne after ref. ⁶⁹. Lowercase letters correspond to principal carbon-isotope peaks identified in the Eastbourne record²⁴. Stratigraphic positions of the Plenus Cold Event (PCE) according to (1) ⁵³, (2)⁷⁰, (3)¹³ with (4) representing supposed PCE position at Cassis. Color-code of the Cassis carbon-isotope record corresponds to lithostratigraphic formations^{22,28} with blue = Grès de l'Anse Sainte Magdeleine Fm., orange = Calcaires du Corton Fm., black = Marnes de l'Anse de l'Arène Fm. Carbon-isotope stratigraphic trend of plant-derived leaf-wax *n*-alkanes (*n*-C₂₅; *n*-C₂₇) is restricted to the Marnes de l'Anse de l'Arène Fm. $\delta^{13}\text{C}$ values of individual *n*-alkanes are the means of duplicate runs ($\sigma = \pm 0.5\text{‰}$) expressed versus VPDB. Gray area represents the stratigraphic interval covered by the OAE2 carbon isotope excursion^{24,54}. Note the expanded thickness of the OAE2 in the Cassis record

Normapolles complex (predominantly *Atlantopollis* and *Complexiopollis* groups; avg. = 18.9%) (Supplementary Fig. 2).

Based on stratigraphic variations in relative spore-pollen abundances, six characteristic assemblage zones (AZ I–VI) are differentiated from base to top (Fig. 3). A pre-CIE assemblage (AZ I, 6.5–18.5 m) shows the lowest number of individual taxa (avg. = 30.2) and a moderately high gymnosperm to angiosperm (G/A) ratio (avg. = 0.65) with the angiosperm component being dominated by non-Normapolles-type pollen. Among conifer pollen, relatively high abundances of *Cerebropollenites* spp. (avg. = 7.3%) are paralleled by low *Inaperturopollenites* spp. content (avg. = 9.5%). The overlying assemblage (AZ II, 34.7–45.2 m) corresponds to the first build-up phase (peak a) of the CIE and shows increased total taxa counts (avg. = 39.9). An increase in Normapolles-type angiosperm pollen results in slightly lower G/A-ratios (avg. = 0.62). Conifer-derived *Inaperturopollenites* spp. remain similar (avg. = 10.6) but show a marked increase toward the top of AZ II reaching up to 22.9%. Above, the trough-shaped CIE interval corresponds to an assemblage (AZ III, 57.1–110.8 m) characterized by stable numbers of taxa (avg. = 40.1) and a low dominance index with average D values of 0.06 indicating a high degree of ecological evenness of the floral association. Increased abundances of Normapolles-type pollen (e.g., *A. microreticulatus*) are paralleled by low conifer pollen contents (e.g., *Inaperturopollenites* spp.) resulting in comparatively low G/A-ratios (avg. = 0.55). The onset of peak (b) is again characterized by an assemblage rich in conifer-derived grains and low angiosperm pollen (AZ IV, 114.2–143.2 m) with increased G/A-ratios (avg. = 0.70) and high dominance index (avg. = 0.09). Another increase in Normapolles-type pollen marks the overlying assemblage (AZ V, 146.3–149.4 m) which shows the lowest

G/A-ratios (avg. = 0.41) paralleled by low D values of 0.06. Above, the upper part of the CIE plateau up to peak (c) corresponds to the topmost assemblage (AZ VI, 156.7–225.3 m). Here, the strong dominance of a few abundant conifer-derived pollen (with *Inaperturopollenites* spp. reaching up to 31.8%; avg. = 20.4%) causes substantially higher G/A-ratios (avg. = 0.77) and higher dominance indices (avg. = 0.12). Calculated origination and extinction records show very low values and the range-through diversity comparatively high and stable values throughout the studied interval, which are illustrating the absence of major land plant extinction during OAE2. Increased values at the base of the origination record and at the top of the extinction record, as well as reduced values at the base and the top of the range-through diversity trend are interpreted as consequences of edge effects.

The overall rich and diverse palynological association obtained from Cassis is taxonomically distinctive for a position within the Late Cretaceous Normapolles phytogeographic province²⁹. Stratigraphic trends in the distribution of the abovementioned groups and indices are considered to primarily reflect changes in the vegetation structure of the adjacent continental hinterland of the SPB.

TEX₈₆ temperature estimates. SST estimates based on TEX₈₆ show continuously high temperatures >35 °C for the SPB during Late Cenomanian–Turonian times with maximum SSTs reaching 38 °C (Fig. 3). These warm SSTs conform with existing TEX₈₆ studies from early Late Cretaceous mid- and low-latitude sites^{5,6,8,9} and highlight the exceptional temperature regime prevailing during deposition of OAE2. A gradual SST decline is

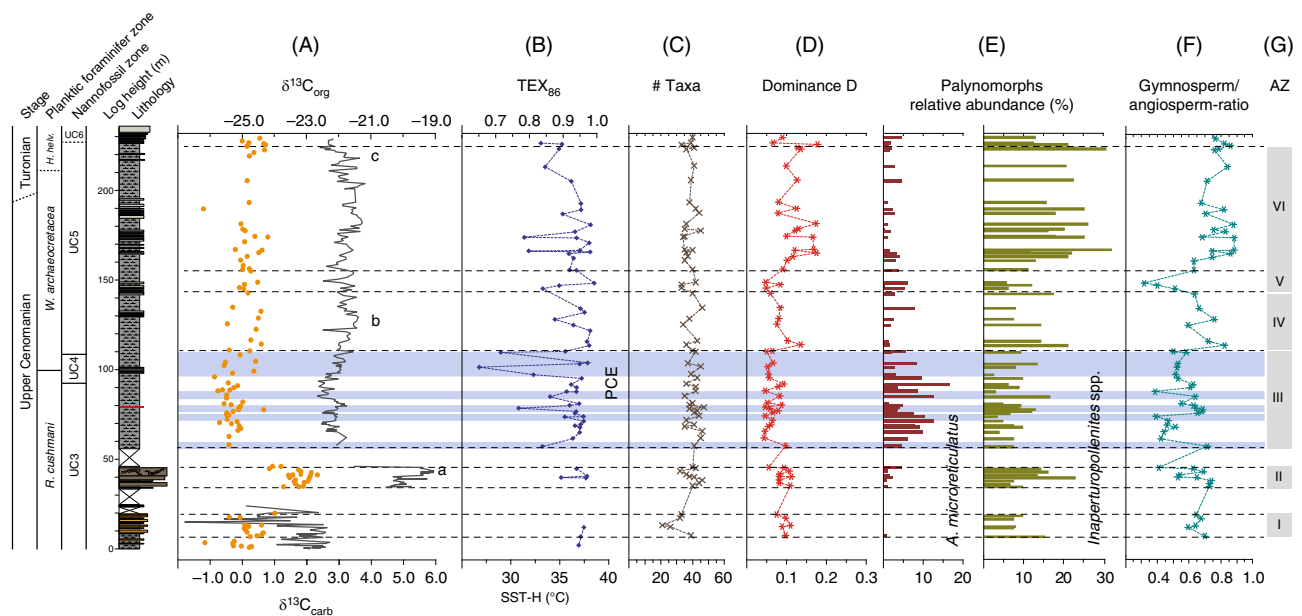


Fig. 3 Terrestrial palynomorph and TEX_{86} data across OAE2. Stratigraphic trends in $\delta^{13}\text{C}_{\text{carb}}$, $\delta^{13}\text{C}_{\text{org}}$, TEX_{86} -derived sea-surface temperatures (SSTs) and evolution of palynofloral diversity and composition across OAE2 at Cassis, S' France. Biostratigraphy and lithological log of Cassis section to the left. **(A)** Carbon-isotope stratigraphy based on bulk rock carbonate and organic matter; **(B)** TEX_{86} and SST reconstruction based on $\text{TEX}_{86}^{\text{H}}$ calibration; **(C)** species richness; **(D)** dominance index; **(E)** stratigraphic distribution of selected pollen including the Normapolles-type angiosperm pollen *Atlantopollis reticulatus* and the conifer pollen *Inaperturopollenites* spp.; **(F)** ratio of gymnosperm versus angiosperm taxa; **(G)** assemblage zones (AZs) based on characteristic spore-pollen associations. PCE = Plenius Cold Event. Blue horizontal bands represent individual SST cooling episodes during the PCE

indicated by decreasing TEX_{86} values characterizing the latest Cenomanian to earliest Turonian at Cassis. In the SPB, the overall pattern of exceptional high temperatures is punctuated by several transient drops towards significantly lower TEX_{86} values (<0.8), which translate into SSTs below 32 °C. These cooler SST estimates characterize a phase of climatic instability and occur within an interval stratigraphically placed within the upper UC3 and UC4 nannofossil zone, below and close to the *R. cushmani*-*W. archaeocretacea* zone boundary and corresponds to the trough-shaped segment of the CIE between peaks (a) and (b).

Discussion

Critically high temperatures have been put forward as a mechanism for the suppression of terrestrial plant and animal life during the end-Permian extinction and basal Triassic events^{30–32}. For these intervals, exceptional climatic warmth is considered a first order control for the well-documented turnover in continental vegetation^{3,33}. During the Cretaceous thermal maximum, exceptional warmth and associated heat stress have also been suggested to significantly affect plant growth by inhibiting photosynthesis to a certain extent at daytime temperatures ranging between 35° and 42 °C²¹. Continental temperatures in this range are considered life-limiting to plants, resulting in serious thermal stress and potential die-off^{34,35}. However, the rich and diverse flora reconstructed from palynological datasets across the OAE2 does not support the idea of widespread heat-induced die-off in continental vegetation—at least not in the hinterland of the studied SPB. Despite maximum TEX_{86} -derived SSTs of up to 38 °C reconstructed for the SPB, the hinterland supported a rich and diverse flora, which is roughly similar in composition to the type of vegetation thriving in Late Cenomanian to Early Turonian times in other parts of the palaeo-European archipelago^{36,37}. Mid-latitude terrestrial plant ecosystems were apparently well adapted to the exceptional warm conditions prevailing during the

Cretaceous thermal maximum. The potential effects of temperature extremes might have been more aggravated in continental interior regions of the subtropics and close to the equator, where even higher mean annual surface temperatures are to be expected³⁸.

Despite the absence of major plant extinction associated with OAE2, variations in the relative contribution of individual taxa and groups reflect compositional changes in vegetation. High contents of Araucariaceae and Cupressaceae-derived pollen indicate the presence of forest communities composed of large trees forming a dense emergent cover^{39,40}. An arborescent habit of Cretaceous araucarioids is supported by abundant fossil wood finds from mid-latitudes⁴¹ and in line with the growth habit of modern *Araucaria* types⁴². Together with high pollen abundances produced by Pinaceae, Podocarpaceae and xerophytic Cheirolepidiaceae, this type of assemblage (AZ II, IV, and VI) is interpreted to reflect mixed forest dominated by arborescent conifers with an only moderate angiosperm component, which grew in mesic habitats with moderate availability of moisture. Such conifer-dominated ecosystems prevailed during episodes of increased $\delta^{13}\text{C}$ values including the first build-up (peak a, AZ II), the second build-up (peak b, AZ IV) and upper plateau phase (AZ VI) of the CIE. During the trough-shaped CIE segment and between peaks b and c, conifer forests were replaced by more diverse, angiosperm-rich vegetation with increased contents of Normapolles-derived pollen (AZ III and V). Late Cenomanian taxa assigned to *Atlantopollis* and *Complexiopollis* are the first representatives of the Normapolles complex^{36,43}, an angiosperm group, which dominated mid-latitude northern hemisphere assemblages during the Late Cretaceous and Early Cenozoic. Based on in-situ findings in fossil flowers, pollen of the Normapolles-type is related to core Fagales⁴⁴. The thick, often multi-layered exine and complex apertures indicate anemophily⁴⁵ and are considered adaptations to open vegetation with widely spaced trees under more dry to seasonally dry climates⁴⁶. During the late Cenomanian, Normapolles-producing angiosperms were probably small non-woody plants or shrubs forming part of a xerophytic savanna-type

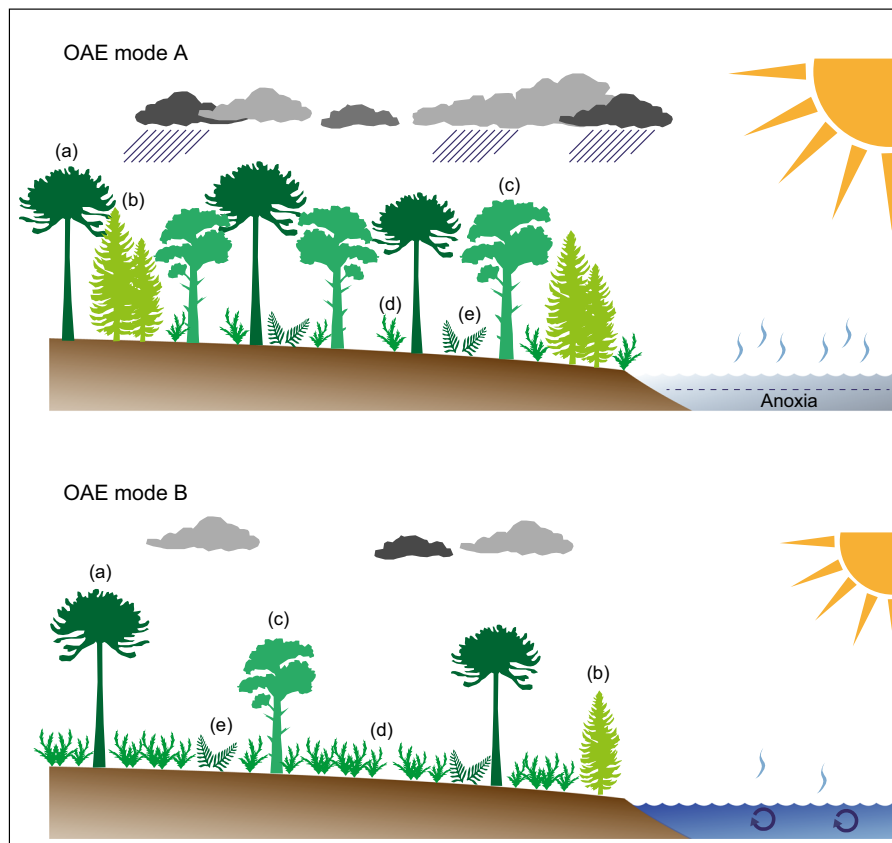


Fig. 4 Tentative changes in mid-latitude vegetation patterns during OAE2. During OAE mode A (e.g. represented by AZ II, IV and VI), the prevailing climate was characterized by exceptional warmth and high moisture availability, giving way to conifer-dominated forests with moderate angiosperm contribution. During OAE mode B (AZ III and V), climatic conditions were cooler and less humid resulting in an open, savanna-type vegetation community with increased abundances of Normapolles-producing angiosperms. (a) Araucariaceae, (b) other conifers incl. Cheirolepidiaceae, (c) Cupressaceae, (d) angiosperms incl. Normapolles-producing forms, (e) ferns

vegetation^{47,48}—a view supported by the rarity of fossil dicot wood in Cenomanian mid-latitude strata from Europe⁴⁹. Accordingly, the palynological record across OAE2 shows changing proportion of arborescent conifer forests (reflecting more mesic conditions) and more open, non-arborescent, angiosperm-rich vegetation.

Fluctuations in the overall climatic patterns during OAE2 have been reported earlier based on marine-derived proxy data. Exceptional climatic warmth associated with OAE2 is considered to have caused accelerated hydrological cycling, enhanced weathering and a generally more humid climate^{9,50–52}. Phases of enhanced moisture availability may have fostered the spread of mesic conifer-dominated forest ecosystems during the onset and later phase of OAE2. Such warm and humid conditions were punctuated by a series of pronounced climatic coolings during the so-called Plenus Cold Event, PCE^{53,54}. The PCE represents a phase of climatic instability and is characterized by several short-lasting SST drops and increases in the range of 2.5–11 °C^{5–13} and paralleled by the southward migration of boreal fauna⁵⁵. Climatic instability was accompanied by a shift towards significantly drier conditions in northern hemisphere mid-latitudes⁹. Stratigraphically, the main pulse of the PCE is located above the first CIE build-up (peak a) at Eastbourne⁵⁴, where it corresponds approximately to the boundary between the *R. cushmani* and *W. archaeocretacea* zones and UC3 to UC4 transition, respectively⁵⁶. At Cassis, the PCE is expressed in a series of several transient drops of TEX₈₆-derived SSTs below 32 °C with the strongest SST decline occurring within the upper part of the CIE trough interval (Fig. 3), similar to what has been observed elsewhere⁵. This part of the CIE with a shift towards lower $\delta^{13}\text{C}$ values has been related

to improved bottom-water oxygenation, enhanced organic carbon remineralization and significant fluctuations in atmospheric $p\text{CO}_2$ ^{13,54,57,58}. In continental mid-latitude settings such as Cassis, this phase of climatic upheaval is characterized by the proliferation of open, savanna-type vegetation rich in angiosperms at the expanse of conifer-dominated forest ecosystems (Fig. 4). Once established, the savanna-type biome was able to persist even during recurrent phases of exceptional warmth in the course of the PCE.

The onset of the Cretaceous thermal maximum including OAE2 took place against the background of a major turnover in global land plant vegetation, namely the rise of angiosperms towards ecological dominance. In mid-latitude settings of North America and Europe, this floral change is marked by the Late Cenomanian radiation of Normapolles-producing plants related to core Fagales^{43,45}. In the Cassis record, early representatives of this group show a pronounced increase in the uppermost Cenomanian assemblage zone III, subsequent to their Mid- to Late Cenomanian origination³⁶. Within the overall warm and humid greenhouse conditions characterizing OAE2, a transient shift towards relatively drier climates and punctuated cooling during the PCE may have fostered a first spread of Normapolles-type angiosperms, which henceforward became a very diverse and successful group dominating mid-latitude plant ecosystems throughout the Late Cretaceous to Early Cenozoic for more than ~50 Ma.

Methods

Stable isotope analyses of carbonate and organic carbon. Measurements of stable carbon and oxygen isotopes of sedimentary carbonates were carried out on

powdered bulk rock material (~0.5 mg) on a total of 292 samples. Stable isotope analysis was conducted using a Thermo Fisher Scientific Gasbench II carbonate device connected to a Thermo Fisher Scientific Delta V Advantage IRMS, available at the Leibniz University Hannover, Germany. The gas bench uses viscous water-free (98 g/mol) orthophosphoric acid at 72 °C to release CO₂ of the calcite from the sample material 1 h before the start of the measurement. Repeated analyses of certified carbonate standards (CO-1, NBS-18, NBS-19) show an external reproducibility $\pm 0.08\text{‰}$ for $\delta^{18}\text{O}$ and $\pm 0.06\text{‰}$ for $\delta^{13}\text{C}_{\text{carb}}$. Values are expressed in conventional delta notation relative to the Vienna-Pee Dee Formation belemnite (VPDB) international standard, in per mil (‰). Stable carbon isotope analyses of bulk organic carbon ($\delta^{13}\text{C}_{\text{org}}$) were performed on 117 decarbonated samples. Powdered samples were treated twice with 6 M HCl for 12 h to remove any carbonate phases and rinsed subsequently with deionised H₂O until neutrality was reached. Stable carbon isotope composition of bulk C_{org} was determined using an organic elemental analyser (Thermo Scientific Flash 2000) connected online to a Thermo Fisher Scientific Delta V Advantage IRMS, available at the Leibniz University Hannover, Germany. The analytical accuracy and reproducibility is checked by replicate analyses of international standards (NBS 22). Reproducibility was better than $\pm 0.1\text{‰}$ for $\delta^{13}\text{C}_{\text{org}}$. Values are expressed in conventional delta notation relative to the Vienna-Pee Dee Formation belemnite (VPDB) international standard, in per mil (‰).

Palynology. A total of 67 rock samples from the Cassis section were prepared for palynological analysis by the Geological Survey of North Rhine-Westphalia in Krefeld, Germany. Cleaned, crushed and weighed samples (20 to 50 g) were treated with 30% HCl and 38% HF for carbonate and silica removal, respectively. Residues were sieved over a 11- μm mesh and mounted on microscope slides, which were analyzed at $\times 200$ and $\times 1000$ magnification. All samples were productive and studied for their particle content (palynofacies) and sporomorph assemblage (spores and pollen), respectively. For the quantification of the spore-pollen assemblage, a minimum of 250 grains were determined per slide (avg. 272 grains) and one entire slide was scanned for rare elements. Five samples did not provide enough sporomorphs to reach the target count of 250 grains. Variations in the spore-pollen assemblage represent normalized frequencies and are reported in percentage [%] of the total assemblage. Thermally unaltered preservation of organic matter is indicated by the virtually unchanged coloring of the sporomorphs and shows a thermal alteration index (TAI) < 2.59 . Preservation of the individual pollen grains varies from moderate to good. Sporomorphs are assigned to floral groups according to their botanical affinity^{60,61}.

Biomarker analysis. For TEX₈₆ analysis, a total of 69 powdered and freeze dried samples (5–10 g dry mass) were extracted with an accelerated solvent extractor, using a 9:1 (v/v) dichloromethane (DCM):MeOH solvent mixture, 3 times for 5 min. at a pressure of ca. 7.6×10^6 Pa and a temperature of 100 °C. The obtained total extracts were rotary evaporated and separated over an activated Al₂O₃ column using 9:1 (v/v) hexane:DCM and 1:1 (v/v) DCM:MeOH solvent mixtures into an apolar and polar fraction, respectively. The polar fraction, containing the glycerol dialkyl glycerol tetraether lipids (GDGTs), was dried under a pure N₂ flow, dissolved ultrasonically in a 99:1 (v/v) hexane:isopropanol mixture at a concentration of 2 mg/ml and filtered over a 0.45 μm mesh PTFE filter (\varnothing 4 mm) prior to HPLC/MS analysis. High-performance liquid chromatography/atmospheric pressure chemical ionization mass spectrometry (HPLC/APCI-MS) analyses was performed on an Agilent 1100 series/Hewlett-Packard 1100 MSD series machine equipped with an auto-injector and HP Chemstation software following⁶².

GDGTs were quantified by integration of peak areas and the TetraEther index of tetraethers composed of 86 carbon atoms (TEX₈₆) was determined⁶³. In order to assess the influence of soil-derived GDGTs on TEX₈₆ values, the BIT index⁶⁴ was applied. Samples with BIT index > 0.3 were excluded from SST reconstruction⁶⁵. Absolute SSTs were reconstructed for 64 samples using TEX₈₆^H core top calibration equations⁶⁶, which has a calibration error of 2.5 °C. The analytical error of TEX₈₆^H-based SST estimates was 0.07 °C based on duplicate analysis. We used the TEX₈₆^H calibration rather than other calibrations⁶⁷ in order to remain consistent with previous literature⁶ and as this has recently been shown to match independent temperature estimates in tropical regions during the Eocene hothouse, the warmest period in the Cenozoic⁶⁸. Although the uncertainty of the calibration used is 2.5 °C, comparisons with other proxy datasets⁶ suggests that TEX₈₆ sometimes can overestimate SSTs, or have a seasonal bias, e.g., toward summer temperatures. Nevertheless, even considering this, the here presented SST estimates of up to 38 °C do suggest hot tropical temperatures well above 30 °C. A level-by-level comparison of TEX₈₆ values and G/A-ratios based on 42 samples supports a general link between SSTs and gross vegetation patterns (Supplementary Fig. 3).

For compound-specific carbon isotope measurements, apolar fractions were treated using an Ag-Silica column with hexane and subsequently ethyl acetate to gain a mostly *n*-alkane pure fraction, which was evaporated under N₂ stream followed by dissolution in 25–50 μl hexane. For measuring the $\delta^{13}\text{C}$ composition of individual *n*-alkanes, 1 ml was injected into the gas chromatograph isotope ratio mass spectrometer (Agilent 6890N GC coupled to a Thermo Delta V advantage IRMS), equipped with a fuse silica capillary column coated with CP-Sil5, with helium used as a carrier gas. The oven was programmed at a starting (injection) temperature of 70 °C, which rose to 130 °C at 20°/min and then 320° at 4°/min, at which it was maintained for 20 min. Values are expressed in conventional delta

notation relative to the Vienna-Pee Dee Formation belemnite (VPDB) international standard, in per mil (‰). All biomarker analyses were carried out at the NIOZ (Royal Netherlands Institute of Sea Research, The Netherlands).

Data availability

All data generated and/or analyzed in this study are included in this published article and its supplementary information file, and are also available from the corresponding author on reasonable request.

Received: 6 February 2018 Accepted: 28 August 2018

Published online: 20 September 2018

References

- Jaramillo, C. et al. Effects of rapid global warming at the Paleocene–Eocene boundary on neotropical vegetation. *Science* **330**, 957–961 (2010).
- McElwain, J., Wade-Murphy, J. & Hesselbo, S. P. Changes in carbon dioxide during an oceanic anoxic event linked to intrusion into Gondwana coals. *Nature* **435**, 479–482 (2005).
- Hochuli, P. A., Sanson-Barrera, A., Schneebeil-Hermann, E. & Bucher, H. Severe crisis overlooked - Worst disruption of terrestrial environments postdates the Permian–Triassic mass extinction. *Sci. Rep.* **6**, 1–7 (2016).
- Norris, R. D., Bice, K. L., Magno, E. A. & Wilson, P. A. Jiggling the tropical thermostat in the Cretaceous hothouse. *Geology* **30**, 299–302 (2002).
- Forster, A., Schouten, S., Moriya, K., Wilson, P. A. & Sinninghe Damsté, J. S. Tropical warming and intermittent cooling during the Cenomanian/Turonian Oceanic Anoxic Event 2: Sea surface temperature records from the equatorial Atlantic. *Paleoceanography* **22**, PA1219 (2007).
- O'Brien, C. L. et al. Cretaceous sea-surface temperature evolution: constraints from TEX₈₆ and planktonic foraminiferal oxygen isotopes. *Earth Sci. Rev.* **172**, 224–247 (2017).
- Voigt, S., Gale, A. S. & Flögel, S. Midlatitude shelf seas in the Cenomanian–Turonian greenhouse world: Temperature evolution and North Atlantic circulation. *Paleoceanography* **19**, PA4020 (2004).
- Sinninghe Damsté, J. S., Van Bentum, E. C., Reichart, G.-J., Pross, J. & Schouten, S. A CO₂ decrease-driven cooling and increased latitudinal temperature gradient during the mid-Cretaceous Oceanic Anoxic Event 2. *Earth. Planet. Sci. Lett.* **293**, 97–103 (2010).
- Van Helmond, Na. G. M. et al. A perturbed hydrological cycle during Oceanic Anoxic Event 2. *Geology* **42**, 123–126 (2014).
- Eldrett, J. S. et al. An astronomically calibrated stratigraphy of the Cenomanian, Turonian and earliest Coniacian from the Cretaceous Western Interior Seaway, USA: implications for global chronostratigraphy. *Cretac. Res.* **56**, 316–344 (2015).
- Li, Y.-X., Montañez, I. P., Liu, Z. & Ma, L. Astronomical constraints on global carbon-cycle perturbation during Oceanic Anoxic Event 2 (OAE2). *Earth. Planet. Sci. Lett.* **462**, 35–46 (2017).
- Schlanger, S. O., Arthur, M. A., Jenkyns, H. C. & Scholle, P. A. The Cenomanian–Turonian Oceanic Anoxic Event, I. Stratigraphy and distribution of organic carbon-rich beds and the marine $\delta^{13}\text{C}$ excursion. *Geol. Soc. Lond. Spec. Publ.* **26**, 371–399 (1987).
- Jarvis, I., Lignum, J. S., Gröcke, D. R., Jenkyns, H. C. & Pearce, M. A. Black shale deposition, atmospheric CO₂ drawdown, and cooling during the Cenomanian–Turonian Oceanic Anoxic Event. *Paleoceanography* **26**, PA3201 (2011).
- Arthur, M. A., Dean, W. E. & Pratt, L. M. Geochemical and climatic effects of increased marine organic carbon burial at the Cenomanian/Turonian boundary. *Nature* **335**, 714–717 (1988).
- Tsikos, H. et al. Carbon-isotope stratigraphy recorded by the Cenomanian–Turonian Oceanic Anoxic Event: correlation and implications based on three key localities. *J. Geol. Soc. Lond.* **161**, 711–719 (2004).
- Fischer, V., Bardet, N., Benson, R. B. J., Arkhangelsky, M. S. & Friedman, M. Extinction of fish-shaped marine reptiles associated with reduced evolutionary rates and global environmental volatility. *Nat. Commun.* **7**, 1–11 (2016).
- Monnet, C. The Cenomanian–Turonian boundary mass extinction (late Cretaceous): new insights from ammonoid biodiversity patterns of Europe, Tunisia and the Western Interior (North America). *Palaeoecol. Palaeoecol.* **282**, 88–104 (2009).
- Jenkyns, H. C. Geochemistry of oceanic anoxic events. *Geochem. Geophys.* **11**, Q03004 (2010).
- Gomez, B. et al. Cretaceous conifers and angiosperms from the Bonarelli Level; reassessment of Massalongo's plant fossil collections of "Monte Colle", Lessini Mountains, northern Italy. *Cretac. Res.* **52**, 179–193 (2015).
- Kuyppers, M. M. M., Pancost, R. D. & Sinninghe Damsté, J. A large and abrupt fall in atmospheric CO₂ concentration during Cretaceous times. *Nature* **399**, 342–345 (1999).

21. Hay, W. W. & Flögel, S. New thoughts about the Cretaceous climate and oceans. *Earth Sci. Rev.* **115**, 262–272 (2012).
22. Jolet, P., Philip, J., Thomel, G., López, G. & Tronchetti, G. Nouvelles données biostratigraphiques sur la limite Cénomanién–Turonien. La coupe de Cassis (Sud-Est de la France): Proposition d'un hypostratotype européen. *Geobios* **34**, 225–238 (2001).
23. Paul, C. R. C. et al. The Cenomanian–Turonian boundary at Eastbourne (Sussex, UK): a proposed European reference section. *Palaeogeog. Palaeoclim. Palaeoecol.* **150**, 83–121 (1999).
24. Jarvis, I., Gale, A. S., Jenkyns, H. C. & Pearce, M. A. Secular variations in late Cretaceous carbon isotopes: a new $\delta^{13}\text{C}$ carbonate reference curve for the Cenomanian–Campanian (99.6–70.6 Ma). *Geol. Mag.* **143**, 561–608 (2006).
25. Floquet, M., Léonide, P., Villier, L., Ackouala, A. P., Blenet, A. Expressions biosédimentaire, diagénétique, géochimique et tectonique de l'événement anoxique Cénomano–Turonien (OAE 2) par les plates-formes carbonatées sud-provençales. Résumé de communication, 13^{ème} Congrès Français de Sédimentologie, Paris (2013).
26. Peyrot, D., Barroso-Barcenilla, F. & Feist-Burkhardt, S. Palaeoenvironmental controls on late Cenomanian–early Turonian dinoflagellate cyst assemblages from Condemios (Central Spain). *Rev. Palaeobot. Palynol.* **180**, 25–40 (2012).
27. Swart, P. K. & Eberli, G. The nature of the $\delta^{13}\text{C}$ of periplatform sediments: Implications for stratigraphy and the global carbon cycle. *Sed. Geol.* **175**, 115–129 (2005).
28. Floquet, M., Gari, J., Hennuy, J., Léonide, P., Philip, J. Sédimentations gravitaires carbonatées et silicoclastiques dans un bassin en transtension, séries d'âge Cénomanién à Coniacien moyen du Bassin Sud-Provençal. *Field guide of the 10^{ème} Congrès Français de Sédimentologie*, 1–80 (2005).
29. Hergreen, G. F. W., Kedves, M., Rovina, L. V., Smirnova, S. B. in *Palynology: Principles and Applications* Vol. 3 (eds Jansonius, J. & McGregor, D. C.) 1157–1188 (AASP Foundation, 1996).
30. Sun, Y. et al. Lethally hot temperatures during the early Triassic greenhouse. *Science* **338**, 366–370 (2012).
31. Cascales-Miñana, B. & Cleal, C. J. The plant fossil record reflects just two great extinction events. *Terra Nova* **26**, 195–200 (2014).
32. Romano, C. et al. Climatic and biotic upheavals following the end-Permian mass extinction. *Nat. Geosci.* **6**, 57–60 (2013).
33. Hermann, E. et al. Terrestrial ecosystems on North Gondwana following the end-Permian mass extinction. *Gondwana Res.* **20**, 630–637 (2011).
34. Berry, J. & Björkman, O. Photosynthetic response and adaption to temperature in higher plants. *Annu. Rev. Plant. Physiol.* **31**, 491–543 (1980).
35. Huber, M. A hotter greenhouse? *Science* **321**, 353–354 (2008).
36. Méon, H., Guignard, G., Pacltová, B. & Svobodová, M. Normapolles. Comparison between central and southwestern Europe during the Cenomanian and Turonian: Evolution of biodiversity and paleoenvironment. *Bull. Soc. Geol. Fr.* **175**, 579–593 (2004).
37. Peyrot, D., Barrón, E., Comas-Rengifo, M. J., Barroso-Barcenilla, F. & Feist-Burkhardt, S. Palynological characterization of the Cenomanian/Turonian boundary at Puentevedey (Burgos, Spain). *Coloq. Pal.* **58**, 101–161 (2008).
38. Poulsen, C. J., Tabor, C. & White, J. D. Long-term climate forcing by atmospheric oxygen concentrations. *Science* **348**, 1238–1241 (2015).
39. Schrank, E. Pollen and spores from the Tendaguru beds, upper Jurassic and lower Cretaceous of southeast Tanzania: palynostratigraphical and palaeoecological implications. *Palynology* **34**, 3–42 (2010).
40. Kershaw, P. & Wagstaff, B. The southern conifer family Araucariaceae: History, status, and value for paleoenvironmental reconstruction. *Annu. Rev. Ecol. Syst.* **32**, 397–414 (2001).
41. Peralta-Medina, E. & Falcon-Lang, H. J. Cretaceous forest composition and productivity inferred from a global fossil wood database. *Geology* **40**, 219–222 (2012).
42. Kunzmann, L. Araucariaceae (Pinopsida): aspects in palaeobiogeography and palaeobiodiversity in the Mesozoic. *Zool. Anz.* **246**, 257–277 (2007).
43. Batten, D. J. Stratigraphic, palaeogeographic and evolutionary significance of late Cretaceous and early Tertiary Normapolles pollen. *Rev. Palaeobot. Palynol.* **35**, 125–137 (1981).
44. Friis, E. M., Pedersen, K. R. & Schönenberger, J. Normapolles plants: a prominent component of the Cretaceous rosoid diversification. *Plant Syst. Evol.* **260**, 107–140 (2006).
45. Friis, E. M., Crane, P. R. & Pedersen, K. R. *Early Flowers and Angiosperm Evolution* (Cambridge Univ. Press, Cambridge, 2011).
46. Wolfe, J. A. & Upchurch, G. R. North American nonmarine climates and vegetation during the late Cretaceous. *Palaeogeog. Palaeoclim. Palaeoecol.* **61**, 33–77 (1987).
47. Wing, S. L. & Tiffney, B. H. The reciprocal interaction of angiosperm evolution and tetrapod herbivory. *Rev. Palaeobot. Palynol.* **50**, 179–210 (1987).
48. Sewall, J. O. et al. Climate model boundary conditions for four Cretaceous time slices. *Clim. Past.* **3**, 647–657 (2007).
49. Philippe, M. et al. Woody or not woody? Evidence for early angiosperm habit from the early Cretaceous fossil wood record of Europe. *Palaeoworld* **17**, 142–152 (2008).
50. Scopelliti, G. et al. High-resolution geochemical and biotic records of the Tethyan 'Bonarelli Level' (OAE2, latest Cenomanian) from the Calabianca-Guidaloca composite section, northwestern Sicily, Italy. *Palaeogeog. Palaeoclim. Palaeoecol.* **208**, 293–317 (2004).
51. Pogge Von, Strandmann, P. A., E., Jenkyns, H. C. & Woodfine, R. G. Lithium isotope evidence for enhanced weathering during Oceanic Anoxic Event 2. *Nat. Geosci.* **6**, 668–672 (2013).
52. Van Helmond, N. A. G. M. et al. Freshwater discharge controlled deposition of Cenomanian–Turonian black shales on the NW European epicontinental shelf (Wunstorf, northern Germany). *Clim. Past.* **11**, 495–508 (2015).
53. Gale, A. S. & Christensen, W. K. Occurrence of the belemnite *Actinocamax plenus* in the Cenomanian of SE France and its significance. *Bull. Geol. Soc. Den.* **43**, 68–77 (1996).
54. Jenkyns, H. C., Dickson, A. J., Ruhl, M. & Van Den Boorn, S. H. J. M. Basalt-seawater interaction, the Plenus Cold Event, enhanced weathering and geochemical change: deconstructing Oceanic Anoxic Event 2 (Cenomanian–Turonian, late Cretaceous). *Sedimentology* **64**, 16–43 (2017).
55. Van Helmond, N. A. G. M. et al. Equatorward phytoplankton migration during a cold spell within the late Cretaceous super-greenhouse. *Biogeosciences* **13**, 2859–2872 (2016).
56. Linnert, C., Mutterlose, J. & Mortimore, R. Calcareous nannofossils from Eastbourne (southeastern England) and the paleoceanography of the Cenomanian–Turonian boundary interval. *Palaios* **26**, 298–313 (2011).
57. Eldrett, J. S., Minisini, D. & Bergman, S. C. Decoupling of the carbon cycle during Ocean Anoxic Event 2. *Geology* **42**, 567–570 (2014).
58. Barclay, R. S., McElwain, J. C. & Sageman, B. B. Carbon sequestration activated by a volcanic CO₂ pulse during Ocean Anoxic Event 2. *Nat. Geosci.* **3**, 205–208 (2010).
59. Staplin, F. L. in *How to Assess Maturation and Palaeotemperatures, SEPM Short Course 7* (ed Staplin, F. L.) 7–31 (Society of Economic Paleontologists and Mineralogists, 1982).
60. Balme, B. E. Fossil in situ spores and pollen grains: an annotated catalogue. *Rev. Palaeobot. Palynol.* **87**, 81–323 (1995).
61. Abbink, O. A., Van Konijnenburg - Van Cittert, J. H. A. & Visscher, H. A sporomorph ecogroup model for the northwest European Jurassic–lower Cretaceous: concepts and framework. *Geol. Mijnb.* **83**, 17–31 (2004).
62. Schouten, S., Hugué, C., Hopmans, E. C., Kienhuis, M. V. M. & Sinninghe Damsté, J. S. Analytical methodology for TEX₈₆ paleothermometry by high-performance liquid chromatography/atmospheric pressure chemical ionization-mass spectrometry. *Anal. Chem.* **79**, 2940–2944 (2007).
63. Schouten, S., Hopmans, E. C., Schefuß, E. & Sinninghe Damsté, J. S. Distributional variations in marine crenarchaeal membrane lipids: a new tool for reconstructing ancient sea water temperatures? *Earth. Planet. Sci. Lett.* **204**, 265–274 (2002).
64. Hopmans, E. C., Weijers, J. W. H., Schefuß, E., Herfort, L. & Sinninghe Damsté, J. S. A novel proxy for terrestrial organic matter in sediments based on branched and isoprenoid tetraether lipids. *Earth. Planet. Sci. Lett.* **224**, 107–116 (2004).
65. Weijers, J. W. H., Schouten, S., Spaargaren, O. C. & Sinninghe Damsté, J. S. Occurrence and distribution of tetraether membrane lipids in soils: Implications for the use of the TEX₈₆ proxy and the BIT index. *Org. Geochem.* **37**, 1680–1693 (2006).
66. Kim, J. H. et al. New indices for calibrating the relationship of the distribution of archaeal isoprenoid tetraether lipids with sea surface temperature. *Geochim. Cosmochim. Acta* **74**, 4639–4654 (2010).
67. Tierney, J. E. & Tingley, M. P. A Bayesian, spatially-varying calibration model for the TEX₈₆ proxy. *Geochim. Cosmochim. Acta* **127**, 83–106 (2014).
68. Evans, D. et al. Eocene greenhouse climate revealed by coupled clumped isotope-Mg/Ca thermometry. *Proc. Natl Acad. Sci. USA* **115**, 1174–1179 (2018).
69. Keller, G., Han, Q., Adatte, T. & Burns, S. J. Palaeoenvironment of the Cenomanian–Turonian transition at Eastbourne, England. *Cretac. Res.* **22**, 391–422 (2001).
70. Voigt, S., Gale, A. S. & Voigt, T. Sea-level change, carbon cycling and palaeoclimate during the late Cenomanian of northwest Europe; an integrated palaeoenvironmental analysis. *Cretac. Res.* **27**, 836–858 (2006).

Acknowledgements

This study was supported by DFG grant HE4467/4-1 and 4-2 to U.H. S.S. was supported by the Netherlands Earth System Science Center funded by the Dutch Ministry of Education, Culture and Science. We gratefully acknowledge Marc Floquet, Katharina Müller, Jean Cors, Pauline Rais, and Alexander Brandt for their assistance during field work in SE France and Christiane Wenske for analytical support. We thank Stefan Huck for comments on an earlier version of the manuscript.

Author contributions

U.H. and T.A. conceived and designed the project with input from S.S. U.H. and T.A. collected the rock samples used in this study. N.W. and U.H. analyzed the palynomorphs

with input from E.S.-H. S.G. and G.K. established the biostratigraphy, S.K. carried out the stable isotope measurements. A.K. carried out the biomarker analyses with the assistance of S.S. U.H. wrote the manuscript with input from all authors.

Additional information

Supplementary Information accompanies this paper at <https://doi.org/10.1038/s41467-018-06319-6>.

Competing interests: The authors declare no competing interests

Reprints and permission information is available online at <http://npg.nature.com/reprintsandpermissions/>

Publisher's note: Springer Nature remains neutral with regard to jurisdictional claims in published maps and institutional affiliations.



Open Access This article is licensed under a Creative Commons Attribution 4.0 International License, which permits use, sharing, adaptation, distribution and reproduction in any medium or format, as long as you give appropriate credit to the original author(s) and the source, provide a link to the Creative Commons license, and indicate if changes were made. The images or other third party material in this article are included in the article's Creative Commons license, unless indicated otherwise in a credit line to the material. If material is not included in the article's Creative Commons license and your intended use is not permitted by statutory regulation or exceeds the permitted use, you will need to obtain permission directly from the copyright holder. To view a copy of this license, visit <http://creativecommons.org/licenses/by/4.0/>.

© The Author(s) 2018